Energy & Environmental Science

RSC Publishing

PAPER

View Article Online
View Journal | View Issue

Phase stability, electrochemical stability and ionic conductivity of the $Li_{10\pm1}MP_2X_{12}$ (M = Ge, Si, Sn, Al or P, and X = O, S or Se) family of superionic conductors†

Cite this: *Energy Environ. Sci.*, 2013, **6**, 148

Shyue Ping Ong,[a] Yifei Mo,[a] William Davidson Richards,[a] Lincoln Miara,[b] Hyo Sug Lee[b] and Gerbrand Ceder*[a]

We present an investigation of the phase stability, electrochemical stability and Li^+ conductivity of the $Li_{10\pm1}MP_2X_{12}$ (M = Ge, Si, Sn, Al or P, and X = O, S or Se) family of superionic conductors using first principles calculations. The $Li_{10}GeP_2S_{12}$ (LGPS) superionic conductor has the highest Li^+ conductivity reported to date, with excellent electrochemical performance demonstrated in a Li-ion rechargeable battery. Our results show that isovalent cation substitutions of Ge^{4+} have a small effect on the relevant intrinsic properties, with $Li_{10}SiP_2S_{12}$ and $Li_{10}SnP_2S_{12}$ having similar phase stability, electrochemical stability and Li^+ conductivity as LGPS. Aliovalent cation substitutions (M = Al or P) with compensating changes in the Li^+ concentration also have a small effect on the Li^+ conductivity in this structure. Anion substitutions, however, have a much larger effect on these properties. The oxygen-substituted $Li_{10}MP_2O_{12}$ compounds are predicted not to be stable (with equilibrium decomposition energies >90 meV per atom) and have much lower Li^+ conductivities than their sulfide counterparts. The selenium-substituted $Li_{10}MP_2Se_{12}$ compounds, on the other hand, show a marginal improvement in conductivity, but at the expense of reduced electrochemical stability. We also studied the effect of lattice parameter changes on the Li^+ conductivity and found the same asymmetry in behavior between increases and decreases in the lattice parameters, *i.e.*, decreases in the lattice parameters lower the Li^+ conductivity significantly, while increases in the lattice parameters increase the Li^+ conductivity only marginally. Based on these results, we conclude that the size of the S^{2-} is near optimal for Li^+ conduction in this structural framework.

Received 15th June 2012
Accepted 1st October 2012

DOI: 10.1039/c2ee23355j

www.rsc.org/ees

Broader context

Solid lithium superionic conductors exhibit good safety and stability, and are promising to replace organic liquid electrolytes in lithium-ion batteries. The current state-of-the-art $Li_{10}GeP_2S_{12}$ superionic conductor has the highest conductivity ever achieved among the solid lithium electrolytes of 12 mS cm^{-1} at room temperature and excellent electrochemical performance. In this work, we attempt to address two key limitations of $Li_{10}GeP_2S_{12}$, namely the high cost of germanium and its air and moisture sensitive sulfide-based chemistry, by studying the phase stability, electrochemical stability and Li^+ conductivity of the $Li_{10\pm1}MP_2X_{12}$ family of superionic conductors (M = Ge, Si, Sn, Al or P, and X = O, S or Se) using first principles calculations. We find that the first limitation can be addressed by substituting relatively cheap silicon or tin for germanium in $Li_{10}GeP_2S_{12}$, with limited impact on stability and conductivity. However, the second limitation cannot be easily addressed by substituting oxide-based chemistry for sulfide-based chemistry; $Li_{10}MP_2O_{12}$ compounds are predicted to be significantly less stable and have lower conductivity than their sulfide counterparts. We also quantify the effect of ion substitutions, lattice parameter changes and Li concentrations on various electrochemical properties, which provides a useful insight into the optimization of LGPS and other similar materials.

Introduction

The continued drive for high performance lithium-ion batteries has imposed stricter requirements on the electrolyte materials.[1] Solid electrolytes comprising lithium superionic conductor materials exhibit good safety and stability, and are promising to replace current organic liquid electrolytes.[2–5] However, one major limitation in the application of Li-ion conductors is that their typical conductivity is less than 10^{-4} S cm^{-1} at room temperature.

In September 2011, Kamaya *et al.* reported a new Li superionic conductor $Li_{10}GeP_2S_{12}$ (LGPS), which has the highest conductivity ever achieved among the solid lithium electrolytes of 12 mS cm^{-1} at room temperature (comparable conductivity with liquid electrolytes), and outstanding electrochemical performance in Li-ion batteries.[6] The high conductivity in LGPS

[a]*Department of Materials Science and Engineering, Massachusetts Institute of Technology, 77 Massachusetts Ave, Cambridge, MA 02139, USA. E-mail: gceder@mit.edu*

[b]*Samsung Advanced Institute of Technology, 1 Cambridge Center, Suite 702, Cambridge, MA 02142, USA*

† Electronic supplementary information (ESI) available. See DOI: 10.1039/c2ee23355j

is attributed to the fast diffusion of Li^+ in its crystal structural framework (see Fig. 1), which consists of $(Ge_{0.5}P_{0.5})S_4$ tetrahedra, PS_4 tetrahedra, LiS_6 octahedra, and LiS_4 tetrahedra. Kamaya *et al.* proposed that diffusion in LGPS occurs along one-dimensional (1D) pathways along the *c*-axis.[6] The authors also proposed that Li atoms in LiS_4 tetrahedra enable fast diffusion along the *c*-direction, while Li atoms in LiS_6 octahedra are not active for diffusion. This hypothetical diffusion mechanism in LGPS has been inferred from the large anisotropic thermal factors and the Li disorder in the 1D channels.

Earlier, we investigated the phase stability, electrochemical stability and Li^+ conductivity of LGPS using first principles techniques.[7] We find that LGPS is a metastable phase in the calculated Li–Ge–P–S phase diagram. We also find that LGPS is not stable against reduction by lithium at low voltage or extraction of Li with decomposition at high voltage. Together with the calculated band gap of 3.6 eV, these predictions suggest that the observed electrochemical window of >5 V for this material is likely the result of a passivation phenomenon, where either Li_2S or P_2S_5 is formed as a decomposition product. Furthermore, while *ab initio* molecular dynamics (MD) simulations confirm fast Li^+ diffusion in the 1D diffusion channel along the *c*-direction, they also predict two additional diffusion pathways in the *a*–*b* plane. Though diffusion in the *a*–*b* plane is not as facile as in the *c*-direction, it nonetheless contributes to the overall performance of the material. A later work by Adams and Prasada Rao[8] using classical MD simulations with a force field based on Morse-type interactions derived from bond valence parameters similarly found weakly anisotropic diffusion in LGPS. In practice, diffusion along more than one dimension is necessary to obtain Li transport over reasonable distances.[9]

Despite its ground-breaking Li^+ conductivity and excellent electrochemical performance, LGPS still suffers from two significant obstacles to its adoption as a solid-electrolyte material. First, there is a practical matter of the use of relatively rare and expensive germanium in LGPS, which would limit large-scale application of the material. Second, sulfide-based compounds tend to be air and moisture sensitive, which could pose problems for cost-effective synthesis and application. These limitations of LGPS motivate us to look for other compounds in the same structural framework that can achieve a better balance between electrochemical performance, cost and other properties.

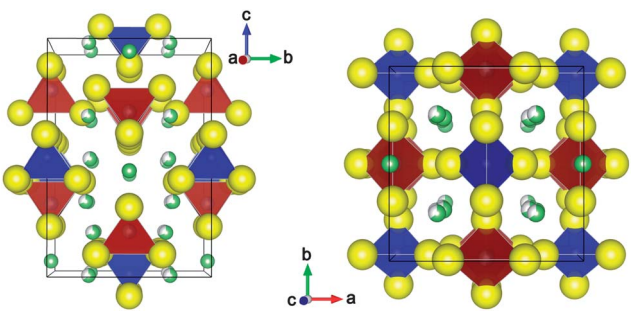

Fig. 1 Crystal structure of $Li_{10}GeP_2S_{12}$. Large yellow atoms: S; small green atoms: fully occupied Li sites; small green-white atoms: partially occupied Li sites; red tetrahedra: $(Ge_{0.5}P_{0.5})S_4$; and blue tetrahedra: PS_4.

In this work, we investigate the phase stability, electrochemical stability and Li^+ conductivity of the $Li_{10\pm1}MP_2X_{12}$ (LMPX) family of superionic conductors, where M = Ge, Si, Sn, Al or P, and X = O, S or Se, using first principles calculations. We seek to elucidate the effect of cation and anion substitutions on these three key properties. We include aliovalent cation substitutions to study the effect of the Li^+ concentration on Li^+ conductivity. We also study the effect of lattice parameters on Li^+ conductivity in the LGPS structural framework.

Methods

All calculations in this work were performed using the Vienna *Ab initio* Simulation Package (VASP)[10] within the projector augmented-wave approach.[11] Given the vastly different requirements of the various techniques used in this paper, we have carefully selected the appropriate functionals and methods for each technique based on accuracy and computational cost considerations, as outlined in the following sections.

Phase stability

The phase stability of the various LMPX structures was investigated by constructing the relevant Li–M–P–X computational phase diagrams.[12,13] To ensure a good coverage of the phase space, we not only included all known Li–M–P–X compounds in the Inorganic Crystal Structure Database,[14] but also included structures derived from the following sources:

(1) All $Li_xP_yS_z$ compounds compiled by Holzwarth *et al.*[15]

(2) All possible inter-substitutions of existing Li–M–X and Li–P–X compounds. For example, the Li–P–O phase space is generally more well-studied than the Li–P–S and Li–P–Se phase space. In fact, some of the $Li_xP_yS_z$ compounds compiled by Holzwarth *et al.*[15] have been obtained by substituting O for S in $Li_xP_yO_z$ compounds. We adopted a similar strategy to ensure a good coverage of all the investigated phase spaces, *e.g.*, we performed O for Se and S for Se substitutions to obtain possible Li–P–Se and Li–M–Se phases.

All total energy calculations for phase stability analysis were performed using the Perdew–Burke–Ernzerhof (PBE) generalized-gradient approximation (GGA)[16] functional. A *k*-point density of at least 500/(number of atoms in the unit cell) was used for all computations. All calculations were spin-polarized.

As the refined LGPS structure ($P4_2/nmc$) has partial occupancies on Li sites as well as Ge/P sites (see Fig. 1),[6] we ordered the arrangement of Li, Ge, and P atoms in LGPS using an electrostatic energy criterion[17] using the Python Materials Genomics (pymatgen) analysis code.[18] All ions were assigned "idealized" charges based on their valence states, *i.e.*, +1 for Li, +4 for Ge, +5 for P and −2 for S. We then selected 30 structures with the lowest electrostatic energy and relaxed them using density functional theory (DFT). It should be noted that the structure that minimizes the electrostatic energy is not the lowest energy structure based on DFT calculations. While the lowest electrostatic energy ordered structure still has a tetragonal $P4_2/mc$ space group, the lowest DFT energy structure has a $P1$ space group with a unit cell that is slightly distorted from the

tetragonal cell (see the ESI† for details). The DFT energy of the relaxed *P*1 structure is approximately 10 meV per atom lower than the DFT energy of the structure that minimizes the electrostatic energy for all the LMPX compounds investigated. Henceforth, we will use the DFT ground state structure of LGPS for the remainder of our analyses. We note that while it is possible that there exist orderings (either for a single unit cell or at larger super cell sizes) that could have lower DFT energies, they are unlikely to be significantly lower in energy. Furthermore, the comparison of phase stability is carried out between materials with similar orderings, and we expect *relative phase stability* to be well characterized even if the exact lowest energy ordering is not obtained. At temperatures of interest (*e.g.*, room-temperature), the Li^+ sites are likely to be disordered, and hence, the structure would have higher symmetry.

All derived isovalent LMPX structures are based on M for Ge and X for S substitution of the DFT ground state structure. For aliovalently substituted structures (Al^{3+} or P^{5+} for Ge^{4+} with corresponding changes in the Li^+ concentration), we performed a similar electrostatic ordering of the structure and then performed DFT calculations on the lowest electrostatic energy structure only, *i.e.*, we did not perform DFT calculations on multiple possible orderings, given the significant computational time involved. Only the sulfide versions of the Al and P structures are investigated in this work. Please see the ESI† for details on the relaxed structures.

Electrochemical stability

We assessed the electrochemical stability of the LMPX compounds using two approaches:

(1) *Intrinsic stability against inert electrodes*. We assessed the intrinsic stability of the LMPX solid electrolyte with respect to inert electrodes by calculating the band gap of the material.[19] As standard semi-local DFT is known to severely underestimate band gaps, the density of states (DOS) of all LMPX compounds were calculated using the Heyd–Scuseria–Ernzerhof (HSE) screened hybrid functional,[20,21] which has been tested to give relatively accurate band gaps for a wide range of materials.[22,23] Owing to the relatively high computational expense of HSE over PBE, non-spin-polarized calculations were performed. The bandgap itself is not an exact measure of the electrochemical stability on inert electrodes as its alignment with respect to an external reference potential is not known. It can, however, be considered as an upper bound for the electrochemical window.

(2) *Chemical stability against electrodes*. We also investigated the chemical stability of the LMPX solid electrolytes against typical electrode materials used in lithium-ion batteries. We constructed the lithium grand potential Li–M–P–X phase diagrams using the method outlined by Ong *et al.*[12,13] Lithium grand potential phase diagrams represent the phase equilibria of a Li–M–P–X system that is open to lithium, which is relevant when the LMPX solid electrolyte is in contact with a reservoir or sink of lithium, as is the case in a lithium battery. The voltage in a battery is the negative of the Li chemical potential. By studying the phase evolution of the $Li_{10\pm1}MP_2X_{12}$ composition with respect to changing lithium chemical potential (μ_{Li}), we can determine the equilibrium phases at μ^0_{Li} corresponding to the bulk metallic lithium (anode) and ($\mu^0_{Li} - 5$) eV corresponding to a 5 V charged cathode. The equilibrium phases provide insight into how sensitive the $Li_{10\pm1}MP_2X_{12}$ composition is to lithium insertion or extraction at high and low voltages and whether the phases formed would affect lithium conductivity. We should note that this analysis pertains to only one possible reaction path with the electrodes, *i.e.*, the exchange of Li between the electrolyte and the electrode. In the case of the cathode, other possible reactions involving non-Li species in the cathode material were not investigated.

Li^+ diffusivity and conductivity

We investigated the Li^+ diffusivity and conductivity in the LMPX materials using *ab initio* molecular dynamics (AIMD) simulations. The AIMD simulations were performed using the PBE GGA functional.[16] To keep the computational cost at a reasonable level, smaller plane wave energy cut-offs of 400 eV, 280 eV and 270 eV were chosen as for oxides, sulfides, and selenides, respectively. A minimal Γ-centered $1 \times 1 \times 1$ *k*-point grid was used, and all calculations were non-spin-polarized.

The AIMD simulations were performed on one unit cell of LMPX. We performed convergence tests on a $2 \times 2 \times 1$ supercell of the original LGPS structure and found that a single unit cell is sufficient to obtain converged diffusivity and conductivity numbers. The volume of the unit cell and the initial position of atoms were obtained from the fully relaxed cells in the phase stability calculations. The integration of Newton's equation is based on the Verlet algorithm implemented in VASP. The time step of molecular dynamics was chosen to be 2 fs. The procedure of the AIMD simulations is as follows:

1. At the start of the MD simulations, the LMPX samples are assigned an initial temperature of 100 K according to a Boltzmann distribution.

2. The samples are then heated up to the desired temperature (600 to 1200 K) by velocity scaling over 1000 time steps (2 ps), and then equilibrated at the equilibrium temperature for 5000 time steps (10 ps) in the NVT ensemble with a constant volume and with a Nosé–Hoover thermostat.[24,25]

3. The MD simulations for diffusion are then performed for 40 ps to 400 ps in the NVT ensemble until the diffusion coefficient is converged. We exclude data points where melting or breaking of M–X bonds is observed.

The diffusion coefficient is defined as the mean square displacement over time:

$$D = \frac{1}{2dt}\left\langle [\boldsymbol{r}(t)]^2 \right\rangle, \quad (1)$$

where d equals to 3, which is the dimension of the lattice in which diffusion takes place. The average mean square displacement $\langle [\boldsymbol{r}(t)]^2 \rangle$ was calculated as:

$$\left\langle [\boldsymbol{r}(t)]^2 \right\rangle = \frac{1}{N}\sum_i \left\langle [\boldsymbol{r}_i(t+t_0)]^2 - [\boldsymbol{r}_i(t_0)]^2 \right\rangle. \quad (2)$$

where $\boldsymbol{r}_i(t)$ is the displacement of the i-th Li ion at time t. The calculated displacement $\boldsymbol{r}_i(t)$ is the displacement of an individual Li atom.

Table 1 Phase equilibria and decomposition energies for $Li_{10\pm1}MP_2X_{12}$

Cation (M)	Anion (X)	Phase equilibria at $Li_{10\pm1}MP_2X_{12}$ composition	E_{decomp} (meV per atom)
Si	O	$Li_4SiO_4 + 2Li_3PO_4$	92
Ge	O	$Li_4GeO_4 + 2Li_3PO_4$	96
Sn	O	$0.33Li_8SnO_6 + 0.67Li_2SnO_3 + 2Li_3PO_4$	97
Si	S	$Li_4SiS_4 + 2Li_3PS_4$	19
Ge	S	$Li_4GeS_4 + 2Li_3PS_4$	25
Sn	S	$Li_4SnS_4 + 2Li_3PS_4$	25
Al	S	$Li_5AlS_4 + 2Li_3PS_4$	60
P	S	$3Li_3PS_4$	22
Si	Se	$Li_4SiSe_4 + Li_4P_2Se_6 + Li_2Se + Se$	16
Ge	Se	$Li_4GeSe_4 + Li_4P_2Se_6 + Li_2Se + Se$	16
Sn	Se	$Li_4SnSe_4 + Li_4P_2Se_6 + Li_2Se + Se$	19

The average mean square displacement is an average over N of all Li ions and is an ensemble average over time t_0. Therefore, the calculated diffusion coefficient D is the self-diffusion of Li^+ ions rather than the combined diffusion of the center of the mass of all Li^+ ions. It is known that these two definitions of diffusion coefficients become equivalent if there is no cross-correlation between displacement $\boldsymbol{r}_i(t)$ of different particles at different times.[26] The value of D is obtained by performing a linear fitting to the relationship of average mean square displacement *versus* $2dt$.

Results

Stability and relaxed structural parameters

Table 1 shows the thermodynamic phase equilibria determined for a $Li_{10\pm1}MP_2X_{12}$ (M = Ge, Si, Sn, Al or P and X = O, S or Se) composition in the Li–M–P–X quaternary phase diagram, as well as the calculated equilibrium decomposition energies (rightmost column). The calculated equilibrium decomposition energy E_{decomp} is a measure of the stability of a material and is defined as the negative of the reaction energy per atom for the $Li_{10\pm1}MP_2X_{12}$ compound to decompose to the predicted thermodynamic equilibrium mixture of stable phases for that composition. Stable materials have an E_{decomp} of 0, and the higher the E_{decomp}, the less likely a structure would be stable. All stable phases in the Li–M–P–X systems investigated are tabulated in the ESI.†

All $Li_{10\pm1}MP_2X_{12}$ compounds are found to be thermodynamically unstable in our calculations. From Table 1, we may identify several clear trends in the stability of the various cation/anion-substituted $Li_{10}MP_2X_{12}$ structures. In general, we find the oxides to be highly unstable in this structure, with E_{decomp} > 90 meV per atom. The sulfide and selenide structures have somewhat similar stability of less than 25 meV per atom, which are sufficiently small that these compounds can be easily stabilized by entropic effects or created as metastable phases. With the exception of the aliovalently substituted $Li_{11}AlP_2S_{12}$, the cation does not seem to significantly affect the stability of the $Li_{10\pm1}MP_2X_{12}$ structure. It may be observed that for the oxides and sulfides in general, the equilibrium phases comprise $Li_4MX_4 + Li_3PX_4$. The only exception is $Li_{10}SnP_2O_{12}$ for which Li_4SnO_4 is unstable *versus* Li_8SnO_6 and Li_2SnO_3. For the selenides, the equilibrium breakdown also contains Li_4MSe_4, but Li_3PSe_4 is unstable against a combination of $Li_4P_2Se_6 + Li_2Se + Se$. $Li_4P_2Se_6$ is a Se-substituted version of the known $Li_4P_2S_6$ compound.[27] We also note that the synthesis of Li_4SnS_4 (isostructural with Li_4GeS_4) has only been reported recently[28] and is indeed predicted to be stable by our calculations.

Table 2 shows the relaxed structural parameters for the $Li_{10}MP_2X_{12}$ compounds investigated. We may observe that the unit cell volumes of $Li_{10}MP_2O_{12}$ compounds are around 53–55% smaller than the corresponding $Li_{10}MP_2S_{12}$ compounds, while the $Li_{10}MP_2Se_{12}$ compounds have unit cell volumes that are around 16–19% larger than the corresponding $Li_{10}MP_2S_{12}$ compounds. A significant proportion of the differences in volume is accounted for by the differences in the anionic radii. The ionic radii of O^{2-}, S^{2-} and Se^{2-} are 126, 170 and 184 pm respectively,[29] which gives $\frac{V_O}{V_S} \approx \left(\frac{r_{O^{2-}}}{r_{S^{2-}}}\right)^3 = 0.40$ and $\frac{V_{Se}}{V_S} \approx \left(\frac{r_{Se^{2-}}}{r_{S^{2-}}}\right)^3 = 1.26$.

We also performed a topological analysis of the relaxed $Li_{10}MP_2X_{12}$ compounds using the open source Zeo++ software.[30,31] For all materials, we removed all Li in the structure and then calculated the largest free sphere that can pass through the structural framework formed by the remaining cations and anions, which is designated as the "channel size" in Table 2. As we can see, the oxide structures tend to have channel sizes that are around 20% smaller compared to the sulfides,

Table 2 Relaxed structural parameters for $Li_{10}MP_2X_{12}$

Cation (M)	Anion (X)	a (Å)	b (Å)	c (Å)	α (°)	β (°)	γ (°)	Volume (Å^3)	Channel size (Å)
Si	O	6.985	6.990	10.649	90.86	89.70	89.88	520	1.43
Ge	O	7.151	6.976	10.709	90.47	89.66	89.81	534	1.46
Sn	O	7.499	6.821	10.966	89.70	90.12	89.35	561	1.50
Si	S	8.566	8.848	12.920	91.90	90.65	90.31	979	1.84
Ge	S	8.561	8.847	12.929	91.97	90.63	90.24	979	1.84
Sn	S	8.666	8.950	13.133	91.97	90.58	90.08	1018	1.86
Al	S	8.722	8.567	13.662	90.69	89.19	89.47	1021	1.92
P	S	8.817	8.817	12.660	90.00	90.00	89.78	984	1.87
Si	Se	9.040	9.381	13.630	91.89	90.74	90.35	1155	1.97
Ge	Se	9.054	9.400	13.690	91.96	90.72	90.31	1164	1.96
Sn	Se	9.084	9.434	13.797	92.09	90.70	90.17	1181	1.97

while the selenides have channel sizes that are around 7% larger. We may also observe that the cation M has a relatively small effect on the size of the channels.

Bandgaps

To evaluate the intrinsic redox stability of the various LMPX compounds, we calculated the density of states (DOS) of all LMPX compounds using the HSE screened hybrid functional. Given that the calculated DOS of all LMPX compounds show similar trends regardless of the cation M, only the calculated DOS for $Li_{10}GeP_2X_{12}$ for X = O, S and Se are shown in Fig. 2. We may make the observation that the O-substituted LMPO materials have a larger bandgap than the LMPS materials, which in turn have a larger bandgap than the Se-substituted LMPSe materials. Furthermore, we also find that both the valence band maximum and the conduction band minimum are dominated by anion states, regardless of the anion chemistry.

The bandgap of a material provides an upper limit on its electrochemical window.[19] The DOS results predict that the O-substituted LMPO materials are expected to have greater intrinsic redox stability than the LMPS compounds, while the Se-substituted compounds are expected to have a lower intrinsic redox stability. This trend can be attributed to the increase in the energy levels of the valence p-orbitals of the anionic species as we move down the periodic table.

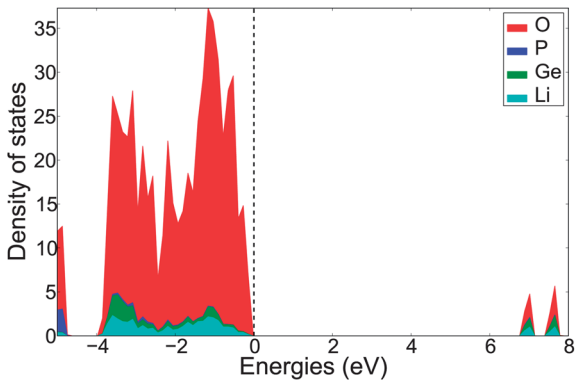

(a) $Li_{10}GeP_2O_{12}$

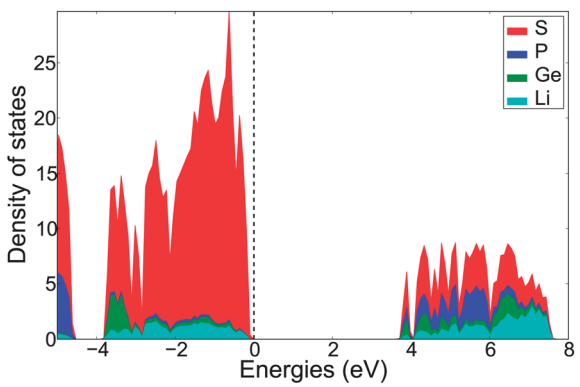

(b) $Li_{10}GeP_2S_{12}$

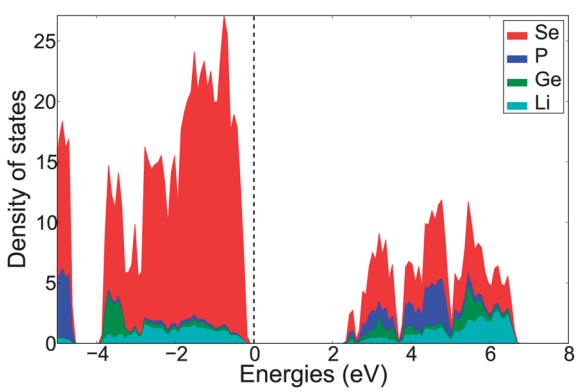

(c) $Li_{10}GeP_2Se_{12}$

Fig. 2 Calculated density of states for $Li_{10}GeP_2X_{12}$ for X = (a) O, (b) S and (c) Se using the HSE screened hybrid functional.

Chemical stability with electrodes

Chemical compatibility between the electrode and the electrolyte is important to prevent capacity degradation and impedance growth. In principle, the electrode material can react with the electrolyte through all of its components, though the reactivity with Li is most critical, as it is, by definition, a mobile species. On the anode side, the chemical potential of Li is very high, and the electrolyte can undergo reduction with Li uptake. The cathode, on the other hand, is strongly oxidizing and can break down the solid electrolyte by extraction of Li.

To investigate the chemical compatibility of LMPX electrolytes under extreme conditions of Li chemical potential, we constructed the lithium grand potential phase diagrams for the Li–M–P–X systems and evaluated the phase equilibria at two extremes for the lithium chemical potential (μ_{Li}): the bulk Li metal chemical potential μ^0_{Li} corresponding to a Li metal anode and $\mu^0_{Li} - 5$ eV corresponding to a charged high-voltage (5 V) cathode.

On the anode, the predicted phase equilibria generally comprise Li_2X, Li_3P and a Li_xM_y alloy. We expect these to have relatively good Li^+ conductivity.[32,33] Hence, while the solid electrolyte is not stable against metallic Li, it is possible to form a conductive solid electrolyte interphase (SEI). However, the presence of metallic products in the decomposition is worrisome and may lead to thickening of this interphase with time.

Table 3 Phase equilibria for the $Li_{10}MP_2X_{12}$ composition at cathode and anode μ_{Li}. The anode μ_{Li} is set at the chemical potential of bulk lithium (μ^0_{Li}), while the cathode μ_{Li} is set at $\mu^0_{Li} - 5$ eV, corresponding to a high voltage 5 V cathode

Cation (M)	Anion (X)	Equilibrium phases at cathode, $\mu_{Li} = \mu^0_{Li} - 5$ eV	Equilibrium phases at anode, $\mu_{Li} = \mu^0_{Li}$
Ge	O	GeP_2O_7, O_2	$Li_{15}Ge_4$, Li_2O, Li_3P
Si	O	SiP_2O_7, O_2	$Li_{21}Si_5$, Li_2O, Li_3P
Sn	O	SnP_2O_7, O_2	$Li_{17}Sn_4$, Li_2O, Li_3P
Ge	S	GeS_2, P_2S_5, S	$Li_{15}Ge_4$, Li_2S, Li_3P
Si	S	SiS_2, P_2S_5, S	$Li_{21}Si_5$, Li_2S, Li_3P
Sn	S	$SnPS_3$, P_2S_5, S	$Li_{17}Sn_4$, Li_2S, Li_3P
Al	S	$AlPS_4$, P_2S_5, S	Li_3Al_2, Li_2S, Li_3P
P	S	P_2S_5, S	Li_2S, Li_3P
Ge	Se	Ge_4Se_9, PSe, Se	$Li_{15}Ge_4$, Li_2Se, Li_3P
Si	Se	$SiSe_2$, PSe, Se	$Li_{21}Si_5$, Li_2Se, Li_3P
Sn	Se	$SnPSe_3$, PSe, Se	$Li_{17}Sn_4$, Li_2Se, Li_3P

On the cathode, however, the phase equilibria are highly dependent on the anion type. The phase equilibria for the oxides at $\mu_{Li}^0 - 5$ eV generally comprise $M_xP_yO_z$ and O_2 gas. This decomposition is likely to lead to significant problems for the long term stability of the electrolyte. For S and Se, the cathodic phase equilibria comprise P_2S_5 and PSe respectively, which may form potentially good glassy ionic conductors and may be passivating (Table 3).[33]

Li^+ diffusivity and conductivity

To elucidate the factors affecting Li^+ diffusivity in the LGPS structural framework, we performed *ab initio* molecular dynamics (AIMD) simulations of various substituted LMPX compounds. Both cation and anion substitutions were investigated. For cation substitutions, we investigated both isovalent as well as aliovalent substitutions with charge neutrality maintained *via* changes in the Li^+ concentration.

Effect of cation substitutions and Li^+ concentration

Fig. 3(a) shows the calculated diffusivities of the isovalent-substituted LMPS structures, where M = Si or Sn. The data for LGPS are included as well for comparison. We may observe that in general, isovalent cation substitutions have a relatively small effect on diffusivity in this structure. The activation energy and Li^+ conductivity at 300 K for all $Li_{10}MP_2S_{12}$ materials are the same within the error of our simulations, as shown in Table 4.

Table 4 Li^+ conductivity of cation-substituted compounds $Li_{10\pm x}MP_2S_{12}$ (M = Si, Sn, P and Al) and anion-substituted compounds $Li_{10}GeP_2X_{12}$ (X = O, S and Se) at 300 K

Compound	E_a (eV)	Conductivity (mS cm^{-1})
$Li_{10}GeP_2S_{12}$	0.21 ± 0.04	13
$Li_{10}SiP_2S_{12}$	0.20 ± 0.03	23
$Li_{10}SnP_2S_{12}$	0.24 ± 0.03	6
$Li_9P_3S_{12}$	0.26 ± 0.09	4
$Li_{11}AlP_2S_{12}$	0.18 ± 0.06	33
$Li_{10}GeP_2O_{12}$	0.36 ± 0.05	0.03
$Li_{10}GeP_2Se_{12}$	0.19 ± 0.04	24

To explore the effect of Li^+ carrier concentration on the diffusivity, we also performed aliovalent cation substitutions, *i.e.*, P^{5+} or Al^{3+} for Ge^{4+} to form $Li_9P_3S_{12}$ or $Li_{11}AlP_2S_{12}$ respectively. While it can be seen from Fig. 3(b) that aliovalent cation substitutions have a slightly larger effect on the diffusivity than isovalent substitution, the calculated data in Table 4 show that the activation barriers and Li^+ conductivities of $Li_9P_3S_{12}$ and $Li_{11}AlP_2S_{12}$ are not significantly different from LGPS based on a *t*-statistic test, which suggests that the effect of carrier

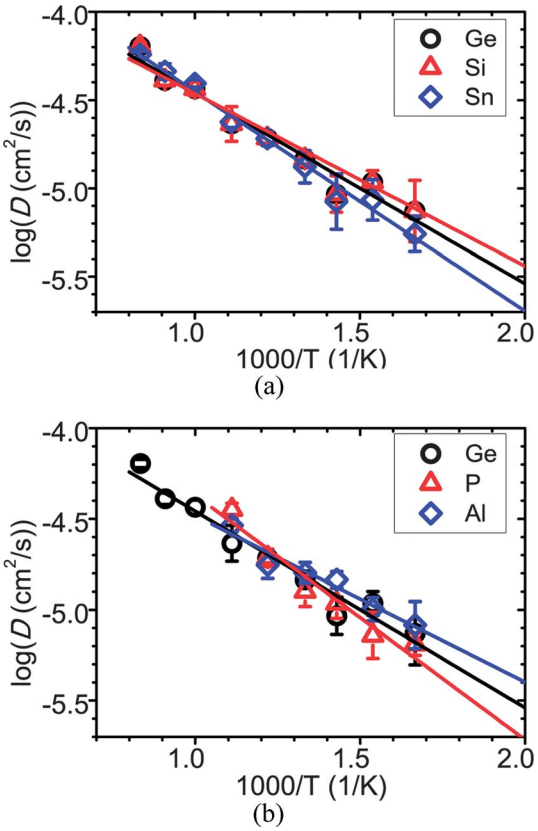

Fig. 3 Effect of (a) isovalent (Si^{4+} and Sn^{4+}) and (b) aliovalent (P^{5+} and Al^{3+}) cation substitutions on diffusivity in the LGPS structure. Data points at 1000 K, 1100 K, and 1200 K are excluded for $Li_{11}AlP_2S_{12}$ and $Li_9P_3S_{12}$ due to melting or breaking of Al–S/P–S bonds in the MD simulations.

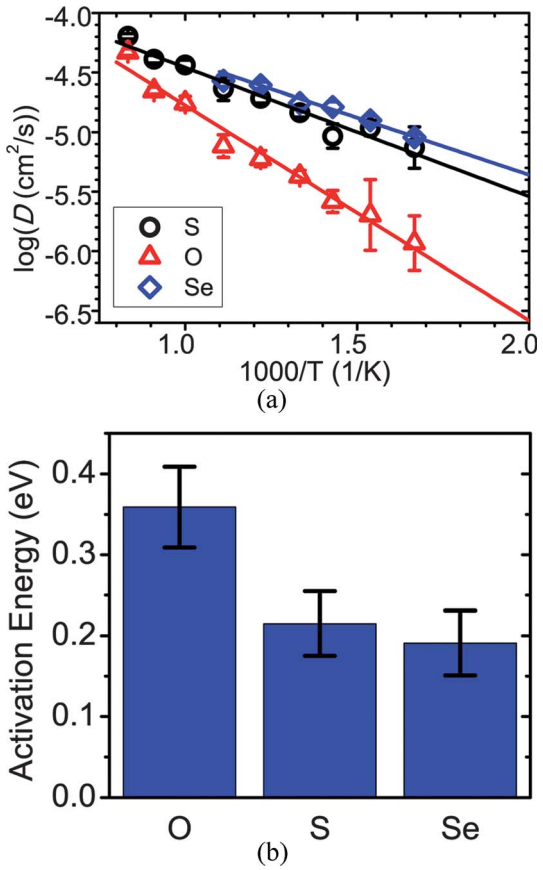

Fig. 4 The (a) diffusivities and (b) activation energies of anion-substituted $Li_{10}GeP_2X_{12}$ (X = O, S, and Se). Data points for diffusivity at 1000 K, 1100 K, and 1200 K for $Li_{10}GeP_2Se_{12}$ have been excluded due to melting in the MD simulations.

concentration and cation substitution is small around the Li^+ concentration of LGPS. The slightly higher Li^+ conductivity and lower activation barrier for $Li_{11}AlP_2S_{12}$ compared to LGPS may be partially accounted for by the larger channel size in this material (Table 2).

Effect of anion substitutions

The calculated diffusivity of $Li_{10}GeP_2X_{12}$ with anion S, O, or Se is shown in Fig. 4. Unlike the case of cation substitutions, we find that anion substitutions in general have a significant effect on Li^+ diffusivity in the LGPX structure. Li^+ diffusivity is significantly slower in $Li_{10}GeP_2O_{12}$ than in $Li_{10}GeP_2S_{12}$. The calculated activation energy of Li^+ diffusion for $Li_{10}GeP_2O_{12}$ of 0.36 eV is also significantly higher than the 0.21 eV of LGPS. As a result, the Li^+ conductivity at 300 K is only 0.03 mS cm^{-1} for $Li_{10}GeP_2O_{12}$, which is three orders of magnitude lower than LGPS. This decrease in Li conductivity is consistent with the general observations that sulfides tend to be much better Li-ion conductors than oxides,[3,34–36] due to the greater size and polarizability of the sulfide anion. A Voronoi analysis of the channel sizes in the LMPX structures (see Table 2) also finds significantly reduced channel sizes in the oxides compared to the sulfides, which could contribute to the observed higher activation energies for oxides.

Based on the comparison between $Li_{10}GeP_2O_{12}$ and LGPS, one may expect that $Li_{10}GeP_2Se_{12}$ has even better diffusivity than LGPS. However, our AIMD simulations show that the Li diffusivity of $Li_{10}GeP_2Se_{12}$ does not improve significantly compared to LGPS. The activation energies for $Li_{10}GeP_2Se_{12}$ and LGPS are the same within the error bar (Table 4). This result suggests that there is a critical diffusion channel size, beyond which Li^+ diffusivity does not improve significantly.

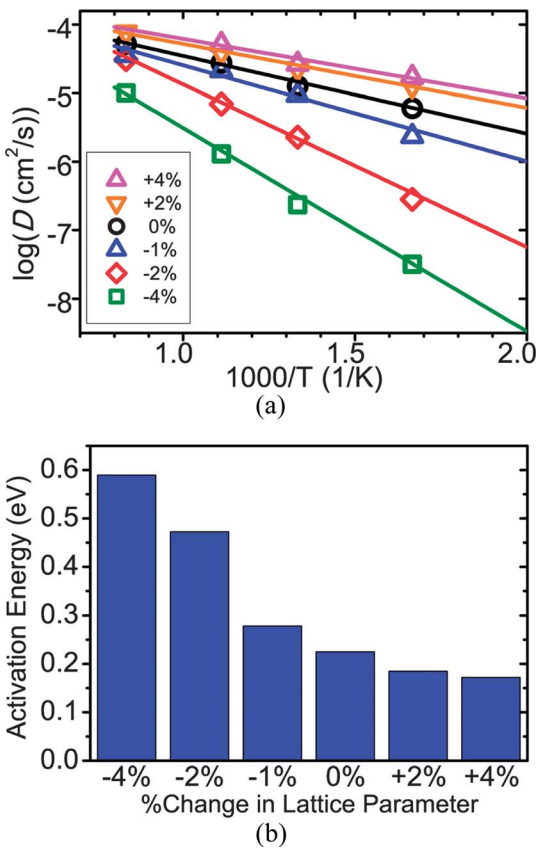

Fig. 5 The (a) diffusivities and (b) activation energies of $Li_{10}GeP_2S_{12}$ with different percentage changes in the lattice parameters.

Table 5 Effect of lattice parameter changes on Li^+ conductivity at 300 K in the LGPS structure

% Change of lattice parameter	E_a (eV)	Conductivity (mS cm^{-1})
−4%	0.59	4.6×10^{-8}
−2%	0.47	4.8×10^{-6}
−1%	0.28	1.7
0%	0.23	13
+2%	0.19	44
+4%	0.17	75

Effect of lattice parameter changes

To investigate the effect of lattice parameter changes on diffusivity in the LGPS structure, we performed AIMD simulations on isotropically scaled LGPS structures for six different scaling factors, ranging from −4% to +4%. Our simulation results (Fig. 5 and Table 5) show that changes in lattice parameters have a significant effect on the Li^+ diffusivity. As the lattice parameters are decreased by 1%, 2%, or 4%, the activation energy increases to 0.28 eV, 0.47 eV and 0.59 eV, respectively. The Li^+ conductivity at room temperature drops by an order of magnitude when the lattice parameters are decreased by 1%, and by more than six orders of magnitude when the lattice parameters are decreased by more than 2%.

On the other hand, when the lattice parameters are increased, we observe a relatively small improvement in the Li^+ diffusivity. Again, this result suggests that the Li diffusion channels in LGPS are already at a somewhat "optimal" size, and further increases in lattice parameters, be it *via* substitution with a larger anion or by artificially increasing the lattice parameters, have a small effect on the Li^+ diffusivity.

Discussion

$Li_{10}GeP_2S_{12}$ (LGPS) has an unusually high Li-ion conductivity, but the use of Ge as a rare and expensive element, and the sulfide anion chemistry make it an unlikely candidate for large-scale application in Li-ion batteries. We investigated the factors influencing stability and diffusivity in the $Li_{10}GeP_2S_{12}$ structure by performing cation and anion substitutions to obtain $Li_{10\pm1}MP_2X_{12}$ compounds. In general, we find that cation substitutions have relatively small effects on stability and diffusivity in this structure, while anion substitutions have a much greater effect.

Oxides are easier to handle than sulfides, but our results indicate that there is little hope for an oxide version of LGPS. We find that while all $Li_{10}MP_2X_{12}$ (M = Ge, Si, or Sn and X = O, S or Se) compounds are thermodynamically somewhat unstable, the

oxides are predicted to be highly unstable with E_{decomp} in excess of 90 meV per atom. The high decomposition energies suggest that an oxide version of the LGPS structure is unlikely to be synthesizable. This may be due to the high stability of Li_3PO_4, which competes for stability with $Li_{10}MP_2O_{12}$ as can be seen from Table 1. Our results further indicate that there would be other problematic issues with $Li_{10}MP_2O_{12}$ electrolytes. We find that the oxygen-substituted $Li_{10}GeP_2O_{12}$ compound has much lower diffusivity (two orders of magnitude) than the LGPS compound, making it considerably less interesting than LGPS. This decrease in diffusivity is most likely due to the much smaller anion radius and polarizability of the oxide anion compared to the sulfide anion; similar observations have been made on the difference in conductivity between the LISICON and thio-LISICON conductors.[35] Finally, our phase stability calculations predict that in contact with cathodes, $Li_{10}MP_2O_{12}$ compounds may undergo Li loss accompanied by the release of O_2 gas, which may prove highly problematic for the long term stability of the electrolyte.

Substituting Se for S only increases the conductivity by a small amount. This is consistent with our investigation of the effect of the lattice parameter on the diffusivity in the LGPS structure: while a decrease in lattice parameters results in significantly lower diffusivity and higher activation barriers, increases in lattice parameters result only in marginally higher diffusivity and marginally lower activation barriers. These observations suggest that the LGPS compound already has somewhat the "ideal" channel size for Li^+ diffusivity in this particular structural framework.

The good news is that cation substitutions of Ge seem to have a very little effect on the performance and stability of LGPS. Neither its Li^+ conductivity nor its anodic and cathodic stabilities are significantly affected. This result may have been expected, given that the interactions between the cations M and Li^+ ions are screened by the S^{2-} anions surrounding the cations. Somewhat surprisingly, we find that aliovalent cation substitutions, with corresponding changes in the Li^+ concentration, also have a relatively small effect on the Li^+ conductivity in the LGPS structure. This is unlike the significant changes in Li^+ conductivity (orders of magnitude) observed in other Li-ion conductors (*e.g.*, lithium lanthanum titanates and NASICON-type materials) with changes in the Li^+ concentration.[2,3] We believe that this is because the $Li_{10}MP_2X_{12}$ composition already has partial occupancies and most of the Li^+ ions are mobile in this structure. Given these data, it seems surprising that so far, no other versions of this compound, other than with Ge, have been reported in the literature.

Finally, a comparison between the DOS in Fig. 2 and the anodic and cathodic decomposition reactions in Table 3 indicates the dangers of assessing the electrochemical stability of potential electrolyte materials based on the intrinsic redox stability alone; chemical compatibility of the electrolyte with electrode materials is an equally important, if not more important, consideration. In terms of redox stability, the HSE-calculated DOS suggest that the oxides would have much better intrinsic redox stability than sulfides and selenides. But while sulfides and selenides form solid reaction products against the cathode and anode, our calculations predict the release of O_2 gas when $Li_{10}MP_2O_{12}$ is in contact with a high voltage cathode, which would be detrimental for stable battery operation.

Conclusions

In conclusion, our investigation of substituted $Li_{10\pm1}MP_2X_{12}$ compounds was motivated by the need to address two key limitations of the LGPS superionic conductor, namely the high cost of germanium, and the air and moisture sensitivity of a sulfide-based chemistry.

Our results show that the first limitation may be addressed by substituting relatively cheap silicon or tin for germanium in this structure. Isovalent cation substitutions have a small effect on the similar phase stability, electrochemical stability and diffusivity in these structures, with similar phase stability, electrochemical stability and Li^+ conductivity predicted for $Li_{12}SiP_2S_{12}$ and $Li_{12}SnP_2S_{12}$ as for LGPS. Aliovalent cation substitutions (M = Al or P) with corresponding changes in the Li^+ concentration also seem to have a small effect on the Li^+ conductivity.

However, the second limitation cannot be addressed by a simple substitution of oxide-based chemistry for sulfide-based chemistry. The oxygen-substituted $Li_{10}MP_2O_{12}$ compounds generally have much worse phase stabilities (with equilibrium decomposition energies >90 meV), better intrinsic electrochemical stabilities and much lower Li^+ conductivity than their sulfide counterparts. The selenium-substituted $Li_{10}MP_2Se_{12}$ compounds show the opposite trend from the oxide materials, but the magnitude of the increase in Li^+ conductivity is much smaller than the decrease in conductivity observed for the oxides. In addition, we also studied the effect of lattice parameter changes on Li^+ conductivity in this material and found the same asymmetry in behavior between increases and decreases in the lattice parameters, *i.e.*, decreases in the lattice parameters lower the Li^+ conductivity significantly, while increases in the lattice parameters increase the Li^+ conductivity only marginally. Based on these results, we conclude that the size of the S^{2-} is near the ideal size for Li^+ conduction in this structural framework.

Acknowledgements

We would like to thank the Samsung Advanced Institute of Technology for their funding support for this research. This research also used computational resources from TeraGrid resources provided by Pittsburgh Supercomputing Center and resources of the National Energy Research Scientific Computing Center, which is supported by the Office of Science of the U. S. Department of Energy under Contract No. DE-AC02-05CH11231.

References

1 M. Armand and J.-M. Tarascon, *Nature*, 2008, **451**, 652–657.
2 S. Stramare, V. Thangadurai and W. Weppner, *Chem. Mater.*, 2003, **15**, 3974–3990.

3 P. Knauth, *Solid State Ionics*, 2009, **180**, 911–916.
4 E. Quartarone and P. Mustarelli, *Chem. Soc. Rev.*, 2011, **40**, 2525–2540.
5 C. Galven, J.-l. Fourquet, M.-P. Crosnier-Lopez and F. Le Berre, *Chem. Mater.*, 2011, **23**, 1892–1900.
6 N. Kamaya, K. Homma, Y. Yamakawa, M. Hirayama, R. Kanno, M. Yonemura, T. Kamiyama, Y. Kato, S. Hama, K. Kawamoto and A. Mitsui, *Nat. mater.*, 2011, **10**, 682–686.
7 Y. Mo, S. P. Ong and G. Ceder, *Chem. Mater.*, 2012, **24**, 15–17.
8 S. Adams and R. Prasada Rao, *J. Mater. Chem.*, 2012, **22**, 7687.
9 R. Malik, D. Burch, M. Bazant and G. Ceder, *Nano lett.*, 2010, **10**, 4123–4127.
10 G. Kresse and J. Furthmuller, *Phys. Rev. B: Condens. Matter Mater. Phys.*, 1996, **54**, 11169–11186.
11 P. E. Blochl, *Phys. Rev. B: Condens. Matter Mater. Phys.*, 1994, **50**, 17953–17979.
12 S. P. Ong, L. Wang, B. Kang and G. Ceder, *Chem. Mater.*, 2008, **20**, 1798–1807.
13 S. P. Ong, A. Jain, G. Hautier, B. Kang and G. Ceder, *Electrochem. Commun.*, 2010, **12**, 427–430.
14 G. Bergerhoff, R. Hundt, R. Sievers and I. D. Brown, *J. Chem. Inf. Model.*, 1983, **23**, 66–69.
15 N. Holzwarth, N. Lepley and Y. a. Du, *J. Power Sources*, 2011, **196**, 6870–6876.
16 J. P. Perdew, M. Ernzerhof and K. Burke, *J. Chem. Phys.*, 1996, **105**, 9982.
17 P. P. Ewald, *Ann. Phys.*, 1921, **64**, 253–287.
18 S. P. Ong, W. D. Richard, A. Jain, G. Hautier, M. Kocher, S. Cholia, D. Gunter, V. L. Chevrier, K. A. Persson and G. Ceder, 2012, submitted.
19 S. P. Ong, O. Andreussi, Y. Wu, N. Marzari and G. Ceder, *Chem. Mater.*, 2011, **23**, 2979–2986.
20 J. Heyd, G. E. Scuseria and M. Ernzerhof, *J. Chem. Phys.*, 2003, **118**, 8207.
21 J. Heyd, G. E. Scuseria and M. Ernzerhof, *J. Chem. Phys.*, 2006, **124**, 219906.
22 J. Heyd and G. E. Scuseria, *J. Chem. Phys.*, 2004, **121**, 1187–1192.
23 T. M. Henderson, J. Paier and G. E. Scuseria, *Phys. Status Solidi B*, 2011, **248**, 767–774.
24 W. Hoover, *Phys. Rev. A: At., Mol., Opt. Phys.*, 1985, **31**, 1695–1697.
25 S. NoseÌĄ, *J. Chem. Phys.*, 1984, **81**, 511.
26 R. Gomer, *Rep. Prog. Phys.*, 1990, **53**, 917–1002.
27 R. Mercier, J. Malugani, B. Fahys, J. Douglade and G. Robert, *J. Solid State Chem.*, 1982, **162**, 151–162.
28 T. Kaib, S. Haddadpour, M. Kapitein, P. Bron, C. S. Der, H. Eckert, B. Roling and S. Dehnen, *Chem. Mater.*, 2012, **8**, 2–10.
29 R. D. Shannon, *Acta Crystallogr., Sect. A: Cryst. Phys., Diffr., Theor. Gen. Crystallogr.*, 1976, **32**, 751–767.
30 R. L. Martin, B. Smit and M. Haranczyk, *J. Chem. Inf. Model.*, 2012, **52**, 308–318.
31 T. F. Willems, C. H. Rycroft, M. Kazi, J. C. Meza and M. Haranczyk, *Microporous Mesoporous Mater.*, 2012, **149**, 134–141.
32 G. Nazri, *Solid State Ionics*, 1989, **34**, 97–102.
33 F. Mizuno, a. Hayashi, K. Tadanaga and M. Tatsumisago, *Adv Mater.*, 2005, **17**, 918–921.
34 B. T. Ahn and R. A. Huggins, *Mater. Res. Bull.*, 1989, **24**, 889–897.
35 R. Kanno, T. Hata, Y. Kawamoto and M. Irie, *Solid State Ionics*, 2000, **130**, 97–104.
36 R. Kanno and M. Murayama, *J. Electrochem. Soc.*, 2001, **148**, A742.

